JNeurosci
THE JOURNAL OF NEUROSCIENCE

Research Articles: Behavioral/Cognitive

Dissecting the function of hippocampal oscillations in a human anxiety model

Saurabh Khemka[1,2], Gareth Barnes[3], Raymond J Dolan[3,4] and Dominik R Bach[1,2,3,4]

[1]*Division of Clinical Psychiatry Research, University of Zurich, 8032 Zürich*
[2]*Neuroscience Centre Zurich, University of Zurich, 8006 Zürich, Switzerland*
[3]*Wellcome Trust Centre for Neuroimaging, University College London, London WC1N 3BG, United Kingdom*
[4]*Max Planck UCL Centre for Computational Psychiatry and Ageing Research, University College London, London WC1N 3BG, United Kingdom*

DOI: 10.1523/JNEUROSCI.1834-16.2017

Received: 7 June 2016

Revised: 5 April 2017

Accepted: 5 May 2017

Published: 16 June 2017

Author contributions: S.K. performed research; S.K., G.B., R.J.D., and D.B. contributed unpublished reagents/ analytic tools; S.K. analyzed data; S.K. and D.B. wrote the paper; G.B., R.J.D., and D.B. designed research.

Conflict of Interest: The authors declare no competing financial interests.

This work was funded by a UCL Neuroscience - Neuroscience Centre Zurich (ZNZ) Collaboration Grant [DRB, RJD], the Wellcome Trust [RJD, Senior Investigator Award 098362/Z/12/Z], and the Medical Research Council [GB, Partnership Grant MR/K005464/1]. The Wellcome Trust Centre for Neuroimaging is supported by core funding from the Wellcome Trust [091593/Z/10/Z]. We thank Raphael Kaplan, Christoph Korn, Vladimir Litvak, Eleanor Loh, Zeb Kurth-Nelson, Matthias Staib, and Athina Tzovara, for their invaluable help and discussions during study design, data collection, and data analysis. The authors declare no competing financial interests.

Corresponding author: Dominik R Bach, Psychiatrische Universitätsklinik Zürich, Lenggstrasse 31, 8032 — Zürich, Switzerland, Email: dominik.bach@uzh.ch

Cite as: J. Neurosci ; 10.1523/JNEUROSCI.1834-16.2017

Dissecting the function of hippocampal oscillations in a human anxiety model

Abbreviated title: Hippocampal oscillations in human anxiety

Saurabh Khemka[1,2], Gareth Barnes[3], Raymond J Dolan[3,4], Dominik R Bach[1-4]

1 Division of Clinical Psychiatry Research, University of Zurich, 8032 Zürich

2 Neuroscience Centre Zurich, University of Zurich, 8006 Zürich, Switzerland

3 Wellcome Trust Centre for Neuroimaging, University College London, London WC1N 3BG, United Kingdom

4 Max Planck UCL Centre for Computational Psychiatry and Ageing Research, University College London, London WC1N 3BG, United Kingdom

Corresponding author: Dominik R Bach

Psychiatrische Universitätsklinik Zürich

Lenggstrasse 31, 8032 – Zürich, Switzerland

Email: dominik.bach@uzh.ch

Number of pages - 35

Number of figures – 5

Number of tables - 2

Number of words: Abstract: 249; Introduction: 450; Discussion: 1254

Acknowledgements: This work was funded by a UCL Neuroscience - Neuroscience Centre Zurich (ZNZ) Collaboration Grant [DRB, RJD], the Wellcome Trust [RJD, Senior Investigator Award 098362/Z/12/Z], and the Medical Research Council [GB, Partnership Grant MR/K005464/1]. The Wellcome Trust Centre for Neuroimaging is supported by core funding from the Wellcome Trust [091593/Z/10/Z]. We thank Raphael Kaplan, Christoph Korn, Vladimir Litvak, Eleanor Loh, Zeb Kurth-Nelson, Matthias Staib, and Athina Tzovara, for their invaluable help and discussions during study design, data collection, and data analysis. The authors declare no competing financial interests.

Abstract

Neural oscillations in hippocampus and medial prefrontal cortex (mPFC) are a hallmark of rodent anxiety models that build on conflict between approach and avoidance. Yet, the function of these oscillations, and their expression in humans, remain elusive. Here, we used magnetoencephalography (MEG) to investigate neural oscillations in a task that simulated approach-avoidance conflict, wherein 23 male and female human participants collected monetary tokens under a threat of virtual predation. Probability of threat was learned beforehand by direct experience. Magnitude of threat corresponded to a possible monetary loss, which was on each trial signalled as a quantity. We focused our analyses on an a priori defined region-of-interest, bilateral hippocampus. Oscillatory power under conflict was linearly predicted by threat probability in a location consistent with right mid-hippocampus. This pattern was specific to hippocampus, most pronounced in gamma band, and not explained by spatial movement or anxiety-like behaviour. Gamma power was modulated by slower theta rhythms, and this theta modulation increased with threat probability. Furthermore, theta oscillations in the same location showed greater synchrony with medial prefrontal cortex theta with increased threat probability. Strikingly, these findings were not seen in relation to an increase in threat magnitude, which was explicitly signalled as a quantity and induced similar behavioural responses as learned threat probability. Thus, our findings suggest that the expression of hippocampal and mPFC oscillatory activity in the context of anxiety is specifically linked to threat memory. These findings resonate with neurocomputational accounts of the role played by hippocampal oscillations in memory.

52 **Significance Statement**

53 We employ a biologically relevant approach-avoidance conflict test in humans whilst
54 recording neural oscillations with magnetoencephalography, in order to investigate the
55 expression and function of hippocampal oscillations in human anxiety. Extending non-human
56 studies, we can assign a possible function to hippocampal oscillations in this task, namely
57 threat memory communication. This blends into recent attempts to elucidate the role of
58 brain synchronisation in defensive responses to threat.

Introduction

Anxiety comprises a suite of behaviours to account for potential threat, enabling an organism to strike a normatively optimal balance in the face of competing goals (Bach, 2015, 2017). Using rodent approach/avoidance conflict tests, such as the elevated plus maze (EPM) or open field test (OFT), a plethora of lesion and drug infusion studies have implicated the ventral hippocampus and medial prefrontal cortex (mPFC) in the control of such behaviours (Gray and McNaughton, 2000; Kjelstrup et al., 2002; Trent and Menard, 2010; Weeden et al., 2015; Ito and Lee, 2016). In line with these findings, a recent lesion study suggested a similar role of the human homologue, the anterior hippocampus, in anxiety-like behaviour (Bach et al., 2014). In rodent anxiety tests, increased ventral hippocampal theta synchronisation with mPFC, and increased theta power in hippocampus, is observed when comparing these situations to a familiar environment (Adhikari et al., 2010; Padilla-Coreano et al., 2016). However, the function of these oscillations and their expression in humans is currently unclear. In this proof-of-principle study, we used an operant conflict test to demonstrate hippocampal power increase in human anxiety and hippocampal synchronisation with mPFC, and to investigate different possible causes.

In rodents, hippocampal and mPFC theta oscillations have been suggested to signal aversive or safe aspects of anxiety situations (Adhikari et al., 2010; Padilla-Coreano et al., 2016). Innate anxiety tests like the EPM or OFT however involve multiple possible threat features, which may be learned in plastic circuits, or hard-wired. This precludes better characterising the function of theta oscillations in these tests. On the other hand, during fear conditioning, a more controlled situation without goal conflict, theta and gamma synchronisation between amygdala, hippocampus and prefrontal cortex has been implicated in the communication of threat memory (Stujenske et al., 2014). Here, we speculated that

hippocampal oscillations, and anxiety-related synchronisation, may preferentially relate to learned threat probability, but not to other aversive features, such as explicitly signalled magnitude of threat.

To this end, we capitalised on a previously established human approach/avoidance conflict model of anxiety (Bach et al., 2014; Korn et al., 2017), embedded in a virtual computer game (Bach, 2015, 2017), while recording magnetoencephalography (MEG) to assess neural oscillations. On each trial of the game, a human player could collect a single monetary token under threat of getting caught by a virtual "predator". Catch probabilities for three distinctly coloured predators were learned by experience beforehand (termed "threat level"). Being caught incurred a monetary loss that was explicitly signalled on each trial (termed "potential loss"). At trial start, the player was presented with the predator colour and the potential loss. After a random interval, the token appeared to create behavioural conflict (Figure 1). We analysed neural oscillations separately at both time points.

Materials and Methods

Datasets. From the student and general population, 20 right-handed healthy participants (mean age ± SD, 24.3 ± 3.91 years; 10 female) were recruited in Zurich for a behavioural experiment (experiment 1), and 25 right-handed healthy participants (22.9 ± 3.68 years; 14 female) took part in a MEG experiment in London (experiment 2). All participants were fluent speakers of German or English, respectively, and had normal or corrected-to-normal vision. Two MEG participants were excluded from the final analysis: one did not complete the experiment and the other made large head movements (> 0.5 cm) impairing source reconstruction.

The study protocol was in full accordance with the Declaration of Helsinki. All participants gave written informed consent after being fully informed about the purpose of the study. The study protocol, participant information, and form of consent, were approved by research ethics committees (Kantonale Ethikkommission Zurich, University College London Research Ethics Committee).

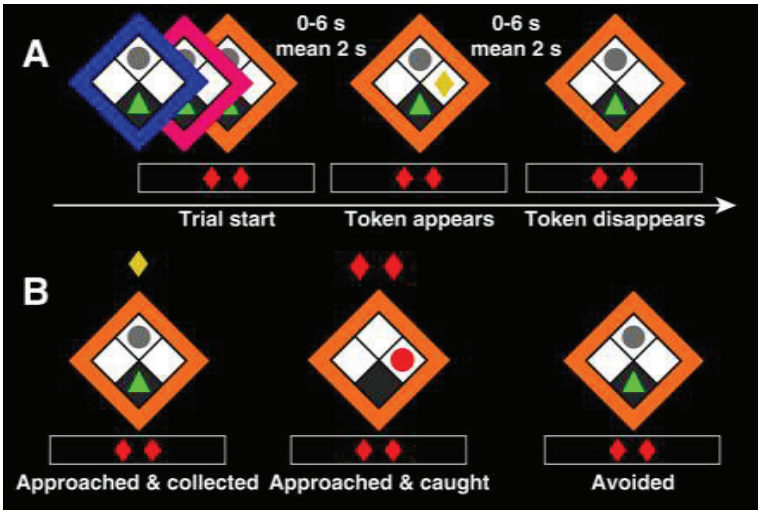

Figure 1. Virtual computer game. (A) At trial start, the player (green triangle) is placed into a "safe place" on a 2x2 grid with one of three different frame colours, representing threat level of a sleeping "predator" (grey circle). Red tokens signal potential token loss upon being caught (0 – 5). After a random interval, a monetary token (yellow diamond) appears. If not collected, it disappears after a random interval. (B) Possible outcomes depend on participants' choice, and chance.

Experimental task. Participants performed an approach-avoidance conflict task (AAC) embedded in a computer game (Figure 1), modified from a previous study (Bach, 2015). Notably, this task involves only financial gains and losses, but previous work indicates that participants' behaviour - in particular the relation of approach latency with expected loss - is not explained by economic theory and fits accounts of anxiety-like behaviour derived from non-human anxiety tasks (Bach, 2015). To make the game usable for MEG, we segregated individual token presentations into separate trials.

On each trial, participants could collect 1 monetary token (approach motivation) under threat of getting caught by a "predator" and consequently losing an explicitly signalled number of tokens (avoidance motivation). Specifically, at the start of each trial (Figure 1A), the human player was in a "safe place", the bottom grid block in a 2x2 diamond grid, and was tasked to decide whether or not to collect a token that would come up in the left or the right grid block. The predator was "sleeping" opposite the safe place, and could become active in a homogenous Poisson process when the human player was outside the safe place, in which case it would catch the player. Three frame colours (blue, pink or orange) represented the threat levels, i.e. the Poisson wake-up rate of the predators. Wake up rates were set to result in a catch probability of 0.1, 0.2, or 0.3, for the three predators, if the player was outside of the safe place for 100 ms, a value established in previous work (Bach, 2015). Threat probabilities were learned by experience beforehand in 36 training trials with zero token loss, which did not count towards the performance-based remuneration. Crucially, threat probabilities were not explicitly instructed. Below the grid, potential loss on the current trial was indicated by red diamonds and varied between 0 and 5.

After a variable time interval, randomly drawn from a gamma distribution with parameters $k = 2$, $\theta = 1$, and mean of 2 s, truncated at 6 s, the token appeared. In case the player did not collect the token, it disappeared after a variable time, drawn from the same distribution, and the trial continued for another 1 s. If the token was collected (Figure 1B), the trial continued until the same pre-determined end time. If the player got caught, it disappeared, the predator turned red and stayed on the screen until the pre-determined end time. The next trial started after a random inter trial interval (ITI) drawn from the same distribution truncated at 4 s, during which the screen was blank. Participants were presented

149 with 648 trials in experiment 1 and 540 trials in experiment 2, evenly distributed across 6
150 different token losses and 3 different threat levels in pseudorandom order.
151 Participant's payment depended on performance in six trials randomly drawn after
152 the experiment and excluding the 36 training trials. The experiment was programmed in
153 Cogent (Version 2000v1.25; www.vislab.ucl.ac.uk/Cogent) under MATLAB 7.14 (Mathworks,
154 Natick, Massachusetts).
155
156 **MEG Data Acquisition.** MEG signals were recorded in a magnetically shielded room with a
157 275-channel Canadian Thin Films (CTF) system with superconducting quantum interface
158 device (SQUID)-based axial gradiometers, a hardware anti-alias filter of 150 Hz cut-off
159 frequency and digitization rate of 600 Hz. Head positioning coils were attached to nasion,
160 left, and right auricular sites, to provide anatomical co-registration, and allowed continuous
161 head localization. Synchronizing markers were written into the MEG data file for precise
162 detection of trial start, token appearance and trial end. A projector displayed the computer
163 game on a screen (~0.8 m distance from the participant). Participants made responses with a
164 button box, and eye blinks were monitored using an eye tracker.
165 This type of MEG system has been successfully used in the past across different
166 laboratories to demonstrate hippocampal oscillations. This includes theta oscillations during
167 navigation, well known from non-human electrophysiology (Cornwell et al., 2012; Kaplan et
168 al., 2012), theta oscillations during memory recall, known from fMRI and animal
169 electrophysiology (Guitart-Masip et al., 2013), hippocampal-mPFC phase coupling during
170 decision making (Guitart-Masip et al., 2013), increased theta oscillations during memory
171 encoding, a phenomenon well known from non-human electrophysiology (Backus et al.,
172 2016), and theta-gamma coupling during replay, another phenomenon from non-human

electrophysiology (Poch et al., 2011). Furthermore, the approach has been used to replicate an fMRI experiment on stimulus novelty, showing increased hippocampal theta oscillations with novelty (Garrido et al., 2015). Simultaneous intracranial EEG and MEG recordings have also provided support for the validity of hippocampal source reconstruction in the gamma band (Dalal et al., 2013). In sum, the gradiometer system appears well suited to record oscillations from hippocampal sources. In terms of theoretic considerations, while there is greater attenuation of distant sources for gradiometers than for magnetometers, this is generally compensated for by an increased SNR due to better noise rejection performance. Under an assumption that the hippocampus is 8 cm away from the nearest sensor, then a 5 cm baseline gradiometer will provide 60% of the signal as compared to a magnetometer. However, at the same time, the gradiometer offers typically a 100-fold improvement in far-field external noise rejection compared to the magnetometer.

Data analysis

Behavioural data analysis. Statistical analysis of behavioural data was carried out in R (www.r-project.org; version 3.1.2). Because the data were unbalanced by design, we used linear mixed effects models (lme4 package) which provide meaningful parameter estimates in this case, using a previously described method (Bach, 2015). All models had the form:

$$\eta \sim \beta_0 + \beta_1 X_1 + \beta_2 X_2 + \beta_3 X_3 + b_k; k = 1..n, b_k \sim N(0, \sigma_b^2)$$

where β_0 is the group intercept, $\beta_{1...3}$ are the fixed effects parameter vectors for 3 threat levels, 6 potential losses, and their interaction, and b_k is the random subject intercept. The linear predictor η is related to the data y through the identity link function for the approach latency data:

$$y_{ijk} \sim N(\eta_{ijk}, \sigma^2 I)$$

and through the logit link function for binary choice choice data (i.e. approach/avoid):

$$y_{ijk} \sim B(1, \frac{1}{1+\exp(\eta_{ijk})}).$$

This is equivalent to the R model formula

$$Y \sim threat\ level * potential\ loss + (1|subject),$$

where Y is the binary choice, or the approach latency. Fixed-effects F-statistics were computed using the R function anova. P-values were calculated using a conservative lower bound on the effective denominator degrees of freedom as

$$df = N - K$$

where N is the number of observations and K is the number of all modelled fixed and random effects. Because the data are unbalanced, i.e. some participants made no approach responses for higher potential loss or threat level, the averaged approach latencies at higher potential loss or threat level will be biased by participants who are more likely to approach. This is why we estimated the approach latency from the model for illustration (lsmeans package). This approach takes the unbalanced dataset into account and estimates the mean approach latency that would be expected in a balanced data set.

MEG data preprocessing. MEG data analysis was conducted in SPM12 (Statistical Parametric Mapping, Wellcome Trust Centre for Neuroimaging, London, UK; *http://www.fil.ion.ucl.ac.uk/spm*). Continuous data from each session were high pass filtered at 0.1 Hz and low pass filtered at 150 Hz using a fifth-order Butterworth filter, down-sampled to 150 Hz, and notch filtered at 50 Hz and 100 Hz to remove mains noise. Data were down sampled to 300 Hz resolution. Epochs from 0-1000 ms relative to trial start and to token appearance of each trial were extracted separately. Epochs in which the interval between trial start and token appearance, or the interval between token appearance and trial end,

were shorter than 1000 ms were discarded from further analysis. This excluded ~26% of the trials as expected from the cumulative density function of the gamma distribution.

Source localization. The linearly constrained minimum variance (LCMV) scalar beamformer spatial filter algorithm (implemented in DAiSS toolbox, *https://github.com/SPM/DAiSS*) was used to generate maps of source activity on a 5 mm grid. Coregistration to the Montreal Neurological Institute (MNI) brain template was based on three fiducial points: nasion, left and right preauricular points. We used a single-shell head model to fit the inner skull surface of the inverse normalized SPM template to more precisely characterize the MEG forward model. The beamformer source reconstruction calculates a set of weights that maps the sensor data to time-series at the source locations. Our broad-band beamforming spatial filters were based on covariance matrix of all trials, in a frequency range of 1-150 Hz and a time window of 0-1000 ms relative to trial start or token appearance.

For each participant, we then created 4 normalized 3D source power images depicting the following contrasts: Difference between high threat and low threat level, linear effect of potential losses across different threat levels, quadratic effect of potential losses across different threat levels and interaction between threat levels and potential losses. The resulting images were smoothed using a Gaussian kernel of 10 mm FWHM (Guitart-Masip et al., 2013). We then performed a second level one-sample t-test on smoothed contrast images from all the participants (df = 22). All statistical parametric maps were thresholded at $p < 0.001$ uncorrected, and small volume corrected for family-wise error at $p < 0.05$ using Gaussian random field theory at the cluster level (Worsley et al., 1996) within the bilateral hippocampus defined by the AAL toolbox (Tzourio-Mazoyer et al., 2002).

239 *Lateralisation.* To assess the laterality of our main finding, we extracted averaged
240 power from the significant clusters and contralaterally mirrored hippocampal regions (i.e.
241 the clusters flipped about the midline). Because this analysis is biased towards exposing a
242 difference, we also extracted data from left and right hippocampus separately. These data
243 were analysed these data in a 3 (threat level) x 2 (hemisphere) ANOVA.

244 *Controlling for behavioural variables.* To exclude that behaviour (decision to
245 approach, or approach latency) explained our findings, we extracted averaged power from
246 both clusters on a trial-by-trial basis. Because behaviour is strongly coupled to threat level
247 and potential loss, the number of instances for each combination of experimental condition
248 and behavioural response is extremely unbalanced. This is why we departed from our
249 previous ANOVA approach and analysed these data in a full hierarchical linear mixed effects
250 model, in line with behavioural data analysis, using the R formula

$$Y \sim behaviour \ * threat\ level * potential\ loss + (1|subject),$$

251 where behaviour corresponds to the approach/avoidance decision (control analysis 1) or to
252 the approach latency (control analysis 2, accounting only for data on trials where
253 participants chose to approach).

254 *Comparing threat level and potential loss.* To compare the effect of threat level and
255 token loss in an unbiased region of interest, we extracted theta power for all trials from all
256 image voxels within the bilateral hippocampus. For each individual voxel and for the average
257 across all voxels, we compared a reduced model containing either the linear effect of threat
258 level together with subject intercepts, or the linear effect of token loss together with subject
259 intercepts. For both models we computed Akaike information criterion (AIC). An absolute
260 AIC difference of > 3 was regarded as decisive (Penny et al., 2004).

261 *Decomposition into frequency bands.* We extracted power from the significant
262 clusters separately for 5 frequency bands: theta (1-8 Hz), alpha (8-12.5 Hz), beta (12.5-30
263 Hz), gamma (30 - 80 Hz), and high gamma (80-150 Hz). To define the frequency range of
264 theta oscillations in humans, we drew on previous work exploring their distinctive
265 association with gamma oscillations at species-specific frequencies. In rodents, these appear
266 to occur between 4-12 Hz (Adhikari et al., 2010). In contrast, intracranial recordings have
267 revealed that human hippocampal theta oscillations occur in an overall lower frequency
268 range (1 – 8 Hz) (Jacobs, 2014). Definition of the other frequency bands was based on
269 conventions in the field.
270 *Time-frequency decomposition.* To analyse the evolution of theta activity at different
271 time points and frequencies, we extracted all sources from the significant cluster and
272 obtained time-frequency decomposition using Morlet-wavelets. We computed mean power
273 per subject and condition for each time point (0 – 1000 ms at 3 ms resolution) and frequency
274 (1 – 150 Hz at 1 Hz resolution). These were then statistically analysed by computing a two-
275 tailed t-test comparing high and low threat level for each data point. To account for multiple
276 comparisons across time points or across frequencies, results were cluster-level corrected
277 using a random permutation test on the trial labels (Maris and Oostenveld, 2007).
278 *Modulation of gamma power envelope:* Gamma power modulation at theta
279 frequency may indicate theta phase/gamma power coupling. To address gamma power
280 modulation, we first averaged power at each time point across the pre-defined gamma band
281 (30-80 Hz) and thus produced a time series of the gamma power envelope for each trial. For
282 this power envelope, we obtained time-frequency decomposition using Morlet-wavelets. We
283 discarded all frequencies above 30 Hz as they have limited interpretability. These data were
284 averaged over time points and trials, for each condition. We then averaged either across all

conditions (overall gamma envelope), or computed the difference between high and low threat. These data were averaged within theta, alpha and beta frequency band, and analysed in a univariate (frequency band) ANOVA, or threat level x frequency band ANOVA. To address evokend (time-locked) modulation of the gamma envelope, we first averaged the gamma envelope within conditions and then repeated this analysis.

Synchronisation analysis: To estimate synchronisation of hippocampal theta oscillations with the rest of the brain, we computed the phase lag index (Stam et al., 2007). We extracted trial-by-trial wise time series for the time window following token appearance, for the first principal component of all sources within the significant cluster (seed source), and then for all other sources in the brain. These time series were filtered (1-8 Hz bidirectional 4th order Butterworth) and Hilbert transformed to compute instantaneous phase $\phi(t,n)$ at time t for source n. Phase lag index was then calculated for each trial as:

$$PLI = \frac{1}{T} \left| \sum_{t=1}^{T} sign[\phi(t, seed) - \phi(t, n)] \right|$$

where $\phi(t, seed)$ represents instantaneous phase of source in the significant cluster at time t. PLI will range from 0 to 1, where a zero PLI indicates no coupling or randomly distributed phase angles and a PLI of 1 indicates constantly positive or negative phase angle across time points and thus tight coupling between two sources of interest. The PLI measure is less prone than other synchronisation measures to the influences of volume conduction from a strong source (Stam et al., 2007; Kaplan et al., 2014). PLI between seed source and any other source in the brain was averaged across trials for each condition, written onto the 5 mm resolution source grid averaged within each condition, and smoothed with a 10 mm FWMH Gaussian kernel before entering them into a second level statistical analysis. Statistical parametric maps were thresholded at $p < 0.001$ uncorrected, and small volume corrected for family-wise error at $p < 0.05$ using Gaussian random field theory at the cluster

level (Worsley et al., 1996) within an anatomical mPFC mask defined by combining BA 8-11, 44-47 in the AAL toolbox (Tzourio-Mazoyer et al., 2002), and restricting this mask to the medial cortex surface (± 4 mm about the midline).

To make plausible that these results are not biased by condition differences in difference phase angle, we extracted for each trial and time point the difference phase angle between seed source and all sources within the significant mPFC cluster from the PLI analysis. This showed no large overall phase angle differences, thus rendering the analysis of PLI unproblematic.

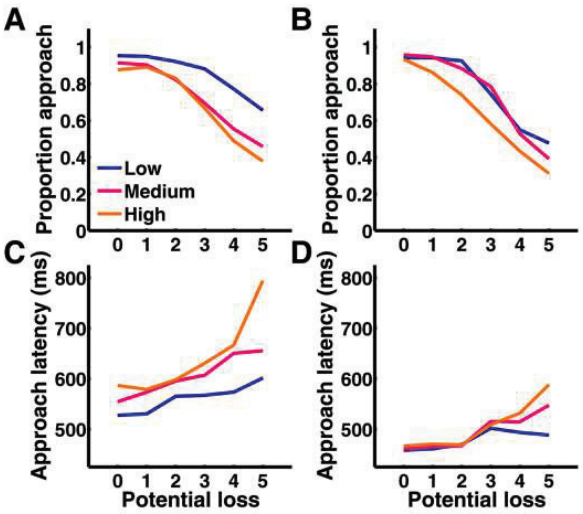

Figure 2. Behavioural results. Proportion of approach responses (AB) and approach latency (CD) for a behavioural experiment (n = 20, AC) and the MEG experiment (n = 23, BD). Approach latency is estimated from a linear mixed effects model to account for the unbalanced data structure.

Results

Increasing threat level, or potential loss, enhances passive avoidance and behavioural inhibition. Figure 2 shows that participants adapted their behaviour across varying level of threat and potential loss in a behavioural control sample, and in the MEG experiment. The proportion of approach responses significantly decreased with increasing threat level, and with potential loss (Figure 2 AB, Table 1), similar to passive avoidance observed in rodents

during anxiety tests. Also, when participants made an approach response, approach latency was longer at high threat level or potential loss (Figure 2 CD, Table 1). This suggests behavioural inhibition relates to expected loss. These results replicate previous reports with a similar operant conflict game in which participants collected tokens cumulatively (Bach, 2015, 2017) whereas here, potential loss did not depend on previous actions. We also noted that participants' behaviour separated between high and low threat situations, but less so between medium and high threat level. A behavioural effect of varying threat level and potential loss on approach latency indicates that our model captures approach-avoidance conflict in humans, and hints at the cross-species comparability of the model.

Hippocampal oscillations relate to threat probability. Upon token appearance, but not at trial start, we observed significantly greater power for high > low threat level in a cluster overlapping with the right mid-hippocampus (Table 2, Figure 3A). We also observed a power decrease for high > low threat level in a cluster overlapping with the left posterior hippocampus and extending into the thalamus (Figure 3B). We extracted power from each cluster and averaged across voxels. For both clusters, power at medium threat level was different from high threat level (one-tailed t-tests, $p < .05$) but not from low threat level ($p > .10$), indicating a non-linearity in the threat level/power relation. However, in a one-way ANOVA, the quadratic term for threat level was not significant ($p > .10$), indicating that this non-linearity may be a chance variation. When comparing the significant clusters to a contralateral region (cluster mask flipped about the midline), we found a significantly greater influence of threat in one hemisphere than in the other. To avoid any bias induced by the cluster-defining contrast, we then extracted power from the anatomical region of interest and averaged separately for each hemisphere. Again, we observed a hemisphere x

threat level interaction for both contrasts (mid-hippocampus $F(1, 44) = 4.04$, $p = .024$; posterior hippocampus $F(1, 44) = 5.55$, $p = .007$; figure 3C). This suggests that the threat-power relationship is truly lateralised. Next, we expanded our field of view and analysed power across the entire brain. No other brain region expressed a power relation with threat level, potential loss, or their interaction, even without correction for multiple comparison.

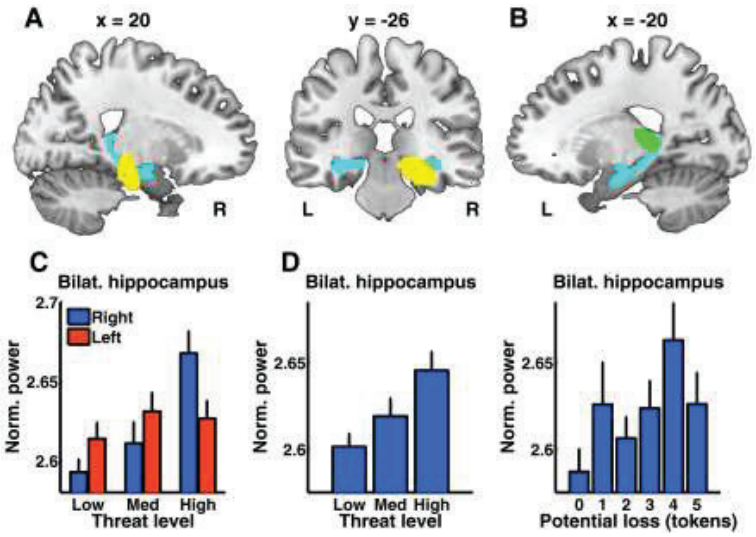

Figure 3. Estimated source power relates to threat level. (A) Right-hemispheric cluster for which estimated power increases with threat level (yellow) within an anatomically defined region of interest (bilateral hippocampus, light blue), visualised on a template brain image ($p < .05$ FWE). (B) Left-hemispheric cluster extending into the tip of the posterior hippocampus for which estimated power decreased with threat level (green). No voxel outside these two clusters showed such relationship at a voxel selection threshold of $p < .001$. (C) Mean normalised power in the hippocampus region of interest, for three different threat levels, shown as condition mean corrected for hemisphere mean across conditions, and SE of difference from participant/hemisphere mean. Power to threat level relation was more pronounced in right than left hemisphere. (D) Mean theta power averaged within the hippocampus region of interest for threat level and potential loss. Data are shown as condition mean, and SE of difference from participant mean.

Hippocampal power and movement. Next, we split our analysis into trials on which the players approached, and trials where they made no movement. Across the brain, we did not find a difference between approach and avoidance trials, neither at trial start nor at token appearance. Because the number of trials is unbalanced for the combinations of

approach/avoidance and threat levels, we extracted power from the significant clusters on a trial-by-trial basis, and analysed these data in a hierarchical linear mixed effects model. This analysis replicated the impact of threat level ($p < .01$ for both clusters) but revealed no effect of approach/avoidance. Next, we included approach latency into a model on trials on which participants approached the token. Approach latency did not relate to power in the mid-hippocampus, but it significantly related to power in the posterior hippocampus ($F(1, 6894) = 6.5$, $p = .01$). However, the effect of threat level was still significant in this analysis ($p < .05$ in both clusters). Taken together, this suggests that the threat level/power relation is not better explained by approach/avoidance, or by approach latency.

Threat level and potential loss. To more directly compare the effects of threat level and token loss, we computed AIC as approximation to the evidence for a model including only threat level, or only potential loss. This analysis was done in the entire anatomical region of interest to avoid any bias induced by the cluster-defining contrast (Figure 3D). Across the bilateral hippocampus, threat level explained more variance than potential loss in power averaged across voxels, and in 50% of individual voxels, while potential loss explained more variance in 2% of voxels. This suggests theta power in the hippocampus is more closely related to threat level than to token loss, as expected from the initial analysis.

Time-frequency decomposition. To decompose the threat level/power relation, we split the beamformer into frequency bands. A threat level x frequency band ANOVA replicated the impact of threat level ($p < .05$ for both clusters) and showed that power was unequally distributed across frequency bands, as expected from their definition ($p < .05$ for both clusters). Notably, we found a threat-level x frequency interaction (mid-hippocampus: $F(8, 176) = 3.32$; $p = .001$; posterior hippocampus: $F(8, 176) = 2.29$; $p = .024$), suggesting that the threat level/power relation was not equally distributed among frequency bands. For the

mid-hippocampus cluster, post-hoc t-tests revealed a significant ($p < .05$) impact of threat level on power in the beta, gamma, and high-gamma band. For the posterior hippocampus cluster, we found an impact of threat level on the theta and gamma band.

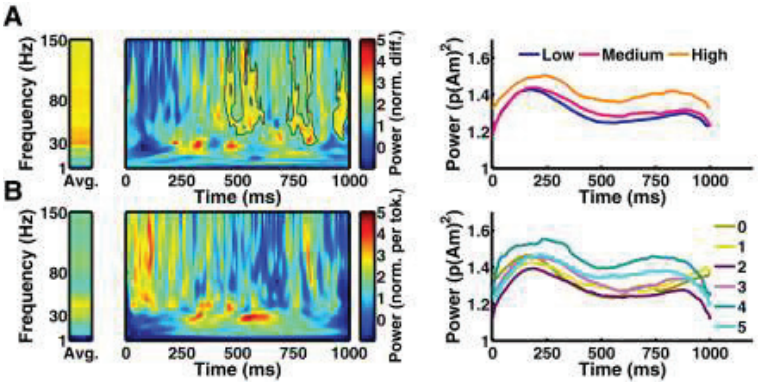

Figure 4. Time frequency decomposition of extracted source activity from mid-hippocampus cluster. (A) Power difference (high vs. low threat) averaged across time points, and for the entire time-frequency window, shown as condition difference normalised by SE of that difference over participants. Significant clusters from a cluster-level permutation test are outlined in black. Time course of power, averaged over all frequencies, is shown in absolute units for the three threat levels. (B) Power increase per additional token, averaged across time points, and for the entire time-frequency window, shown as regression slope normalised by the SE of that regression slope over participants. Time course of power, averaged over all frequencies, is shown in absolute units for the six potential losses.

We then extracted the estimated time course of all sources within the significant clusters, and computed a time-frequency decomposition. Statistical contrasts were corrected for multiple comparison using a cluster-level permutation test. In the mid-hippocampus cluster, an impact of threat level was particularly pronounced above 25 Hz and after about 450 ms, (Figure 4A). Cluster-level tests on averages across time, or frequencies, revealed that the effect of threat level was particularly pronounced at frequencies between 23-150 Hz, and for all time points between 297-900 ms. For the posterior hippocampus cluster, this analysis revealed no clusters of interest.

Theta modulation of gamma power

For the remaining analyses, we focused on the mid-hippocampus cluster which is spatially close to, and shows the same threat/power relation as, the ventral hippocampus subregion for which previous rodent work has revealed oscillatory coupling. Extracted gamma power from this cluster appeared to be modulated by lower frequencies (Figure 4A), reminiscent of a theta phase/gamma power coupling observed in rodent anxiety models (Stujenske et al., 2014). To analyse this modulation, we averaged gamma (30-80 Hz) power for each point in time, and analysed spectral modulation (1-30 Hz) of this gamma power envelope for each trial (Figure 4C). Averaged within frequency bands, this analysis revealed overall stronger modulation of gamma power envelope in theta/alpha than in beta band (main effect frequency, $F(2, 44) = 11.46$, $p < .001$, post hoc test theta > beta band: $t(22) = 3.65$, $p = .001$; alpha > gamma band: $t(22) = 3.70$, $p = .001$). Furthermore, gamma envelope appeared to be particularly more modulated at theta/alpha than at beta frequencies when threat level was high (interaction threat level x frequency, $F(2, 44) = 4.94$, $p = .012$, post hoc test theta > beta band: $t(22) = 2.29$, $p = .032$; alpha > beta band: $t(22) = 2.30$, $p = .030$). Strikingly, when first averaging gamma envelope within conditions and then doing the spectral decomposition, we found the same pattern of results. This suggests theta/alpha modulation of gamma power is time-locked to token presentation.

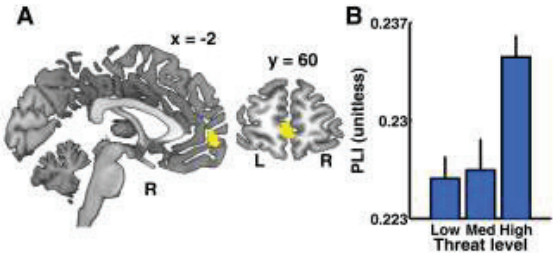

Figure 5. Phase coupling of mid-hippocampus cluster with mPFC. (A) At token appearance, PLI between mid-hippocampus and mPFC increases with threat level. Significant cluster (yellow, region BA10) overlayed on a template brain image ($p < .05$, cluster level corrected for family wise error in a mPFC mask as defined in the AAL toolbox). (B) Mean PLI value in the significant cluster for three different threat levels, corrected for medium threat level. PLI is shown as condition mean/SE of difference from participant mean.

Theta synchronisation between mPFC and hippocampus. Finally, based on previous findings that hippocampal and mPFC theta oscillations synchronise more strongly when threat is higher, we computed the phase lag index (PLI) between the maximum source in the mid-hippocampus cluster, and all other sources in the brain, and analysed the resulting PLI images. While there was no impact of potential loss on PLI, we found an mPFC area for which PLI increased with higher threat level ($p < 0.05$; cluster-level corrected for family-wise error within anatomically defined mPFC; Figure 5AB; Table 2). This result appeared to reflect phase coupling and was not driven by differences in mean phase angle between the two conditions.

Discussion

Neural oscillations in hippocampus, and hippocampus/mPFC theta synchronisation is often observed in rodent approach/avoidance conflict tests of anxiety. In the present study, we investigated occurrence and synchronisation of hippocampal oscillations in humans, to elucidate their possible role in behavioural control during approach/avoidance conflict.

As a first result, we show that hippocampal power is linearly predicted by learned threat probability, but not by explicitly signalled threat magnitude, two prominent aversive features in this approach/avoidance conflict test. The locations of the significant MTL clusters were consistent with mid-hippocampus (positive relation to threat probability) and posterior tip of hippocampus (negative relation to threat probability). Crucially and extending previous studies, this finding cannot be explained by behavioural reponses, i.e. the initiation and latency of virtual movements. While in the rodent model, theta and gamma oscillations have been linked to aversive and safe features of a situation (Likhtik et al., 2014; Stujenske et al., 2014), our results are more specific and restrict the relevant aversive features to threat probability. Because threat probability is learned in our task, and threat magnitude is explicitly signalled to participants on each trial, this may suggest that a possible function of hippocampus in this task is restricted to situations involving retrieval of threat memories. This result resonates with results from more restricted experiments involving threat memory, namely fear conditioning. Here, amygdala/mPFC synchronisation appears to signal threat memory (Likhtik et al., 2014). It has been further shown that optogenetic inhibition of basolateral amygdala projection terminals in the animals' ventral hippocampus disrupts anxiety-like behaviours, suggesting that hippocampus may be interacting with amygdala to receive threat related memories (Felix-Ortiz et al., 2013). Interestingly, in our data set, hippocampal responses are only seen when a token appeared to create behavioural conflict, but not at trial start when all features of the situation were already signalled. This may indicate that the hippocampus is specifically involved in monitoring behavioural conflict, including a retrieval of threat memory (Oehrn et al., 2015; Ito and Lee, 2016).

We can rule out that our results relate to conflict alone because threat magnitude and threat probability both share a relation with conflict, but only probability relates to hippocampal power. Also, by removing most spatial features from the paradigm used in the current study, we are able to firmly rule out that the treat probability/hippocampal power relation is related to an impact of spatial navigation. As a limitation, while the location of the significant MTL cluster is consistent with the mid-hippocampus, more precise MEG methods may be required to corroborate the exact location within the MTL. Furthermore, the cluster was not significant in a whole-brain analysis. While we had strong a priori reasons to focus on the hippocampus as region of interest, replication with high-precision MEG (Troebinger et al., 2014a; Troebinger et al., 2014b) could possibly strengthen this finding.

Interestingly, the threat level/power relationship was most pronounced in the gamma band. Hippocampal gamma oscillations are often coupled to theta phase (Lisman and Jensen, 2013), as also shown with MEG (Poch et al., 2011). However, there is a sparsity of rodent literature on this coupling in approach/avoidance conflict. It appears that rodent amygdala gamma power is coupled to either local or mPFC theta rhythms, depending on threat (Stujenske et al., 2014). However, amygdala gamma power in this previous study showed a negative relation to threat, and may thus be distinct from the gamma power effects we observe here. Crucially, we find stronger theta modulation of hippocampal gamma power when threat is higher, suggesting theta/gamma coupling.

Finally, we identify a positive relation of hippocampal/mPFC coupling with threat level, i.e. hippocampal and mPFC rhythms appear more synchronised when threat is higher. This is in keeping with rodent findings (Adhikari et al., 2010; Padilla-Coreano et al., 2016), which we crucially extend by demonstrating the lack of a relation between potential loss and hippocampus/mPFC coupling. This may indicate that this coupling is intricately linked to a

situation in which threat memories are retrieved. A difference in our report from findings using optogenetic manipulations in rodents (Padilla-Coreano et al., 2016) is that we did not assess directionality of this coupling. Interestingly, the location of mPFC coupling with hippocampus in BA10 reflects an area found to synchronise with hippocampus during value-based decision-making (Guitart-Masip et al., 2013).

In a different human approach/avoidance test involving spatial navigation ("stay and play" game), we have previously shown that hippocampal blood oxygenation measured by functional magnetic resonance imaging relates to threat level (Bach et al., 2014), just like hippocampal oscillatory power in the current study. The power effect in the current study was broadly limited to gamma band (24-150 Hz), and oscillations in this frequency range show a robust relationship with BOLD responses (Boorman et al., 2015; Hutchison et al., 2015; Scheeringa et al., 2016), rendering the two findings rather consistent. Interestingly, other fMRI studies on anxiety-like behaviour in approach/avoidance conflict have also suggested an encoding of conflict per se and/or action tendencies in multivariate patterns of hippocampal BOLD signal (O'Neil et al., 2015; Loh et al., 2016). Control analyses of our data revealed that such features were not represented in hippocampal power, or hippocampal/mPFC coupling in our task. Interestingly, both of these latter studies addressed a slightly different situation, in which a decision is being abstractly communicated to the computer via button press, while the motor execution of that button press has no impact on outcome. Our initial "stay and play" task (Bach et al., 2014), as in most rodent anxiety tests, required specific motor behaviours. While largely removing the element of spatial navigation in our current task, motor execution is still crucial and has a major impact on outcomes: if players move later they are less likely to obtain the token; if the return to the safe place later they are more likely to get caught. This task demand may rely on partly distinct neural

534 control than the more abstract demands in (O'Neil et al., 2015; Loh et al., 2016) which share
535 some analogy with specific operant rodent tests (Geller and Seifter, 1960; Vogel et al., 1971).
536 Indeed, using similar operant conflict tests, a more recent rodent and (human and non-
537 human) primate literature has not implicated the hippocampus in approach/avoidance
538 decision making at all, and rather highlighted contributions of anterior cingulate, and of
539 striosomes in the basal ganglia (Amemori and Graybiel, 2012; Amemori et al., 2015;
540 Aupperle et al., 2015; Friedman et al., 2015). However, as a limitation to this distinction, a
541 role of the anterior cingulate rather than hippocampus has also been highlighted in an
542 approach/avoidance task with naturalistic continuous responses (Gonen et al., 2016).
543 Reconciling spatial, mnemonic, conflict processing, and behavioural control functions of the
544 hippocampus will therefore require more elaborated experimental scenarios (Ito and Lee,
545 2016).
546 To summarise, we employed a virtual computer game simulating biologically relevant
547 approach-avoidance conflict in humans, to investigate functional role of hippocampal
548 oscillations. We show that hippocampal power linearly relates to learned threat probability
549 in a location consistent with the right mid-hippocampus. This is not paralleled by threat
550 magnitude, and cannot be explained by virtual movement, action tendencies, or conflict per
551 se. This result mainly appears to stem from the gamma band, which shows stronger theta
552 modulation when threat is higher. Finally, theta oscillations in this location are more
553 synchronised with mPFC at higher threat probability. Thus it appears that the role of
554 hippocampal oscillations and their synchronisation with mPFC in approach/avoidance
555 situations is restricted to the retrieval of threat memory. This resonates with recent
556 attempts to elucidate the role of brain synchronisation in defensive behaviour.
557

558 **References**

559
560 Adhikari A, Topiwala MA, Gordon JA (2010) Synchronized activity between the ventral
561 hippocampus and the medial prefrontal cortex during anxiety. Neuron 65:257-269.

562 Amemori K, Amemori S, Graybiel AM (2015) Motivation and affective judgments
563 differentially recruit neurons in the primate dorsolateral prefrontal and anterior
564 cingulate cortex. J Neurosci 35:1939-1953.

565 Amemori KI, Graybiel AM (2012) Localized microstimulation of primate pregenual cingulate
566 cortex induces negative decision-making. Nat Neurosci 15:776-785.

567 Aupperle RL, Melrose AJ, Francisco A, Paulus MP, Stein MB (2015) Neural substrates of
568 approach-avoidance conflict decision-making. Human brain mapping 36:449-462.

569 Bach DR (2015) Anxiety-Like Behavioural Inhibition Is Normative under Environmental
570 Threat-Reward Correlations. PLoS computational biology 11:e1004646.

571 Bach DR (2017) The cognitive architecture of anxiety-like behavioral inhibition. J Exp Psychol
572 Hum Percept Perform 43:18-29.

573 Bach DR, Guitart-Masip M, Packard PA, Miro J, Falip M, Fuentemilla L, Dolan RJ (2014)
574 Human Hippocampus Arbitrates Approach-Avoidance Conflict. Current Biology
575 24:541-547.

576 Backus AR, Schoffelen JM, Szebenyi S, Hanslmayr S, Doeller CF (2016) Hippocampal-
577 Prefrontal Theta Oscillations Support Memory Integration. Current biology : CB
578 26:450-457.

579 Boorman L, Harris S, Bruyns-Haylett M, Kennerley A, Zheng Y, Martin C, Jones M, Redgrave P,
580 Berwick J (2015) Long-latency reductions in gamma power predict hemodynamic
581 changes that underlie the negative BOLD signal. J Neurosci 35:4641-4656.

582 Cornwell BR, Arkin N, Overstreet C, Carver FW, Grillon C (2012) Distinct contributions of
583 human hippocampal theta to spatial cognition and anxiety. Hippocampus 22:1848-
584 1859.

585 Dalal SS, Jerbi K, Bertrand O, Adam C, Ducorps A, Schwartz D, Garnero L, Baillet S, Martinerie
586 J, Lachaux JP (2013) Evidence for MEG detection of hippocampus oscillations and
587 cortical gamma-band activity from simultaneous intracranial EEG. Epilepsy &
588 Behavior 28:310-311.

589 Felix-Ortiz AC, Beyeler A, Seo C, Leppla CA, Wildes CP, Tye KM (2013) BLA to vHPC inputs
590 modulate anxiety-related behaviors. Neuron 79:658-664.

591 Friedman A, Homma D, Gibb LG, Amemori K, Rubin SJ, Hood AS, Riad MH, Graybiel AM
592 (2015) A Corticostriatal Path Targeting Striosomes Controls Decision-Making under
593 Conflict. Cell 161:1320-1333.

594 Garrido MI, Barnes GR, Kumaran D, Maguire EA, Dolan RJ (2015) Ventromedial prefrontal
595 cortex drives hippocampal theta oscillations induced by mismatch computations.
596 NeuroImage 120:362-370.

597 Geller I, Seifter J (1960) A Conflict Procedure for the Evaluation of Drugs. Fed Proc 19:20-20.

598 Gonen T, Soreq E, Eldar E, Ben-Simon E, Raz G, Hendler T (2016) Human mesostriatal
599 response tracks motivational tendencies under naturalistic goal conflict. Social
600 cognitive and affective neuroscience:nsw014.

601 Gray JA, McNaughton N (2000) The neuropsychology of anxiety: An enquiry into the
602 functions of the septohippocampal system. Oxford, UK: Oxford University Press.

603 Guitart-Masip M, Barnes GR, Horner A, Bauer M, Dolan RJ, Duzel E (2013) Synchronization of
604 medial temporal lobe and prefrontal rhythms in human decision making. J Neurosci
605 33:442-451.

606 Hutchison RM, Hashemi N, Gati JS, Menon RS, Everling S (2015) Electrophysiological
607 signatures of spontaneous BOLD fluctuations in macaque prefrontal cortex.
608 NeuroImage 113:257-267.

609 Ito R, Lee ACH (2016) The role of the hippocampus in approach-avoidance conflict decision-
610 making: Evidence from rodent and human studies. Behavioural Brain Research
611 313:345-357.

612 Jacobs J (2014) Hippocampal theta oscillations are slower in humans than in rodents:
613 implications for models of spatial navigation and memory. Philosophical transactions
614 of the Royal Society of London Series B, Biological sciences 369:20130304.

615 Kaplan R, Doeller CF, Barnes GR, Litvak V, Duzel E, Bandettini PA, Burgess N (2012)
616 Movement-related theta rhythm in humans: coordinating self-directed hippocampal
617 learning. PLoS Biol 10:e1001267.

618 Kaplan R, Bush D, Bonnefond M, Bandettini PA, Barnes GR, Doeller CF, Burgess N (2014)
619 Medial prefrontal theta phase coupling during spatial memory retrieval.
620 Hippocampus 24:656-665.

621 Kjelstrup KG, Tuvnes FA, Steffenach HA, Murison R, Moser EI, Moser MB (2002) Reduced fear
622 expression after lesions of the ventral hippocampus. ProcNatlAcadSciUSA 99:10825-
623 10830.

624 Korn CW, Vunder J, Miro J, Fuentemilla L, Hurlemann R, Bach DR (2017) Amygdala lesions
625 reduce anxiety-like behavior in a human benzodiazepine-sensitive
626 approachavoidance
627 conflict test. Biological psychiatry in press.

628 Likhtik E, Stujenske JM, M AT, Harris AZ, Gordon JA (2014) Prefrontal entrainment of
629 amygdala activity signals safety in learned fear and innate anxiety. Nat Neurosci
630 17:106-113.

631 Lisman JE, Jensen O (2013) The theta-gamma neural code. Neuron 77:1002-1016.

632 Loh E, Kurth-Nelson Z, Berron D, Dayan P, Duzel E, Dolan R, Guitart-Masip M (2016) Parsing
633 the Role of the Hippocampus in Approach-Avoidance Conflict. Cereb Cortex.

634 Maris E, Oostenveld R (2007) Nonparametric statistical testing of EEG- and MEG-data. J
635 Neurosci Methods 164:177-190.

636 O'Neil EB, Newsome RN, Li IHN, Thavabalasingam S, Ito R, Lee ACH (2015) Examining the
637 Role of the Human Hippocampus in Approach–Avoidance Decision Making Using a
638 Novel Conflict Paradigm and Multivariate Functional Magnetic Resonance Imaging.
639 The Journal of Neuroscience 35:15039-15049.

640 Oehrn CR, Baumann C, Fell J, Lee H, Kessler H, Habel U, Hanslmayr S, Axmacher N (2015)
641 Human hippocampal dynamics during response conflict. Current Biology 25:2307-
642 2313.

643 Padilla-Coreano N, Bolkan SS, Pierce GM, Blackman DR, Hardin WD, Garcia-Garcia AL,
644 Spellman TJ, Gordon JA (2016) Direct Ventral Hippocampal-Prefrontal Input Is
645 Required for Anxiety-Related Neural Activity and Behavior. Neuron 89:857-866.

646 Penny WD, Stephan KE, Mechelli A, Friston KJ (2004) Comparing dynamic causal models.
647 NeuroImage 22:1157-1172.

648 Poch C, Fuentemilla L, Barnes GR, Duzel E (2011) Hippocampal theta-phase modulation of
649 replay correlates with configural-relational short-term memory performance. J
650 Neurosci 31:7038-7042.

651 Scheeringa R, Koopmans PJ, van Mourik T, Jensen O, Norris DG (2016) The relationship
652 between oscillatory EEG activity and the laminar-specific BOLD signal.
653 ProcNatlAcadSciUSA 113:6761-6766.

654 Stam CJ, Nolte G, Daffertshofer A (2007) Phase lag index: assessment of functional
655 connectivity from multi channel EEG and MEG with diminished bias from common
656 sources. Human brain mapping 28:1178-1193.

657 Stujenske JM, Likhtik E, Topiwala MA, Gordon JA (2014) Fear and safety engage competing
658 patterns of theta-gamma coupling in the basolateral amygdala. Neuron 83:919-933.

659 Trent NL, Menard JL (2010) The ventral hippocampus and the lateral septum work in tandem
660 to regulate rats' open-arm exploration in the elevated plus-maze. Physiol Behav
661 101:141-152.

662 Troebinger L, Lopez JD, Lutti A, Bestmann S, Barnes G (2014a) Discrimination of cortical
663 laminae using MEG. NeuroImage 102 Pt 2:885-893.

664 Troebinger L, Lopez JD, Lutti A, Bradbury D, Bestmann S, Barnes G (2014b) High precision
665 anatomy for MEG. NeuroImage 86:583-591.

666 Tzourio-Mazoyer N, Landeau B, Papathanassiou D, Crivello F, Etard O, Delcroix N, Mazoyer B,
667 Joliot M (2002) Automated anatomical labeling of activations in SPM using a
668 macroscopic anatomical parcellation of the MNI MRI single-subject brain.
669 NeuroImage 15:273-289.

670 Vogel JR, Beer B, Clody DE (1971) Simple and Reliable Conflict Procedure for Testing Anti-
671 Anxiety Agents. Psychopharmacologia 21:1-&.

672 Weeden CS, Roberts JM, Kamm AM, Kesner RP (2015) The role of the ventral dentate gyrus
673 in anxiety-based behaviors. Neurobiology of learning and memory 118:143-149.

674 Worsley KJ, Marrett S, Neelin P, Vandal AC, Friston KJ, Evans AC (1996) A unified statistical
675 approach for determining significant signals in images of cerebral activation. Human
676 brain mapping 4:58-73.

677
678

679 **Figure legends**

680 **Figure 1. Virtual computer game.** (A) At trial start, the player (green triangle) is placed into a
681 "safe place" on a 2x2 grid with one of three different frame colours, representing threat
682 level of a sleeping "predator" (grey circle). Red tokens signal potential token loss upon being
683 caught (0 – 5). After a random interval, a monetary token (yellow diamond) appears. If not
684 collected, it disappears after a random interval. (B) Possible outcomes depend on
685 participants‘ choice, and chance.

686

687 **Figure 2. Behavioural results.** Proportion of approach responses (AB) and approach latency
688 (CD) for a behavioural experiment (n = 20, AC) and the MEG experiment (n = 23, BD).
689 Approach latency is estimated from a linear mixed effects model to account for the
690 unbalanced data structure.

691

692 **Figure 3. Estimated source power relates to threat level.** (A) Right-hemispheric cluster for
693 which estimated power increases with threat level (yellow) within an anatomically defined
694 region of interest (bilateral hippocampus, light blue), visualised on a template brain image ($p < .05$ FWE). (B) Left-hemispheric cluster extending into the tip of the posterior hippocampus
696 for which estimated power decreased with threat level (green). No voxel outside these two
697 clusters showed such relationship at a voxel selection threshold of $p < .001$. (C) Mean
698 normalised power in the hippocampus region of interest, for three different threat levels,
699 shown as condition mean corrected for hemisphere mean across conditions, and SE of
700 difference from participant/hemisphere mean. Power to threat level relation was more
701 pronounced in right than left hemisphere. (D) Mean theta power averaged within the

hippocampus region of interest for threat level and potential loss. Data are shown as condition mean, and SE of difference from participant mean.

Figure 4. Time frequency decomposition of extracted source activity from mid-hippocampus cluster. (A) Power difference (high vs. low threat) averaged across time points, and for the entire time-frequency window, shown as condition difference normalised by SE of that difference over participants. Significant clusters from a cluster-level permutation test are outlined in black. Time course of power, averaged over all frequencies, is shown in absolute units for the three threat levels. (B) Power increase per additional token, averaged across time points, and for the entire time-frequency window, shown as regression slope normalised by the SE of that regression slope over participants. Time course of power, averaged over all frequencies, is shown in absolute units for the six potential losses.

Figure 5. Phase coupling of mid-hippocampus cluster with mPFC. (A) At token appearance, PLI between mid-hippocampus and mPFC increases with threat level. Significant cluster (yellow, region BA10) overlayed on a template brain image ($p < .05$, cluster level corrected for family wise error in a mPFC mask as defined in the AAL toolbox). (B) Mean PLI value in the significant cluster for three different threat levels, corrected for medium threat level. PLI is shown as condition mean/SE, of difference from participant mean.

723 **Tables**

724 **Table 1.** Effect of threat level, potential loss and their interaction on proportion of approach
725 responses, and approach latency in control and MEG study, as estimated in a linear mixed
726 effects model on single trial data.

	F	p	df
Effect on approach responses			
Behavioural experiment 1 (n = 20)			
Threat level	109.14	< .001	2, 12276
Potential loss	346.78	< .001	5, 12276
Threat level x Potential loss	1.67	0.08	10, 12276
MEG experiment 2 (n = 23)			
Threat level	27.85	< .001	2, 12380
Potential loss	438.78	< .001	5, 12380
Threat level x Potential loss	7.18	< .001	10, 12380
Effect on approach latency			
Behavioural experiment 1 (n = 20)			
Threat level	29.42	< .001	2, 9268
Potential loss	42.69	< .001	5, 9268
Threat level x Potential loss	4.65	< .001	10, 9268
MEG experiment 2 (n = 23)			
Threat level	3.54	.029	2, 9082
Potential loss	20.84	< .001	5, 9082
Threat level x Potential loss	2.29	.019	10, 9082

727

728

729 **Table 2.** MEG findings. Results are cluster-level corrected for family wise error within the
730 anatomically defined region of interest (bilateral hippocampus or bilateral mPFC), at $p < 0.05$
731 (cluster defining threshold of $p < 0.001$). Coordinates and peak z-values refer to overall peak
732 of the unmasked cluster.
733

	Hemisphere				Cluster size (mm^3)	Overlap with ROI mask (mm^3)	Peak z-value
		x	y	z			
Token appearance: High threat > Low threat							
Mid-hippocampus	R	20	-24	-16	6256	1088	3.60
Posterior hippocampus/Thalamus	L	-12	-30	4	3504	464	4.18
Token appearance, phase lag index with respect to averaged sources in intermediate hippocampus cluster: High threat > Low threat							
Medial frontal gyrus (BA 10)	bilateral	-2	60	0	744		3.40

734